Surface Science 650 (2016) 130–139

Contents lists available at ScienceDirect

Surface Science

journal homepage: www.elsevier.com/locate/susc

Cluster formation and distributions in field ionization of coadsorbed methanol and water on platinum

C.J. Rothfuss [a], V.K. Medvedev [a,b], E.M. Stuve [b,*]

[a] PO Box 1791, Laramie, WY 82073, United States
[b] Department of Chemical Engineering, Box 351750, University of Washington, Seattle, WA 98195-1750, United States

ARTICLE INFO

Available online 24 December 2015

Keywords:
Methanol
Water
Field ionization
Pulsed field desorption
Platinum
Ion clusters

ABSTRACT

Pure and mixed clusters of methanol and water were examined with pulsed field desorption time-of-flight mass spectrometry (TOF-MS) as a function of adlayer composition varying from pure water to nominally pure methanol. The experiments were performed on a Pt tip at 165 K and total pressure of approximately 5×10^{-6} Torr. Protonated clusters of up 7 water molecules and up to 4 methanol molecules were detected. For mixed adlayers, mixed clusters involving 1 or 2 water and methanol molecules were observed. The hydronium cluster $(H_2O)H^+$ exhibited unusual behavior in that its maximum intensity occurred for an approximately equimolar mixture. This was attributed to direct ionization of a methanol monohydrate species, $(CH_3OH{\cdot}H_2O)$. Water production was observed in methanol-rich layers and ascribed to scission of the C–O bond to produce CH_3 and OH. The TOF-MS data exhibited significant time lags for most higher mass clusters. The time lags for pure H_2O were analyzed in terms of a two-step mechanism involving a trade-off of ion cluster emission and growth, from which the rate constant for cluster growth was estimated as 9×10^{-6} s^{-1}.

Published by Elsevier B.V.

1. Introduction

The nature and production of solvated ions are important factors in a wide variety of processes, such as electrochemistry, corrosion, and biochemistry. In a proton conducting fuel cell, for example, adsorbed hydrogen desorbs from the anode to form a solvated proton

$$H_{ads} + n\ \ H_2O_{elyte} \rightarrow (H_2O)_n H^+_{elyte} + e^- \quad (1)$$

that migrates to the cathode. The subscript "elyte" refers to the electrolyte phase. This reaction consists of an adsorbed H atom interacting with n water molecules, simultaneously transferring an electron to the metal. This is, literally, the electricity producing step in a fuel cell. The details of this step – how charge transfer and solvation of the proton occur – depend on the electrocatalytic nature of the electrode. Hydrogen solvation with charge transfer has been detected in ultrahigh vacuum studies. The reaction proceeds on high work function Pt surfaces [1–3], but has not been detected on others.

Electrocatalysis involves the combined aspects of surface chemistry and surface electric field effects. Surface reactions, such as hydrogen adsorption or oxygen adsorption (with or without dissociation) depend primarily on surface chemistry. The surface electric field exists nearby, but outside of, the surface and can alter the kinetic rate constants of: (i) ion adsorption and desorption, (ii) solvation of desorbing species, (iii) desolvation of adsorbing species, and (iv) interactions of ions with adsorbates. At the potential of zero charge, the surface electric field is the nascent field of the metal interacting with a medium of zero net charge. Other potentials, positive or negative, cause positive or negative changes in the surface electric field. The surface electric field can vary within the range of ± 0.5 V/Å, as determined by the Gouy-Chapman model of the double layer. Electric fields in this range are large enough to induce many reactions [4] and ionize H_2O to a series of protonated clusters $(H_2O)_nH^+$. In fact, the pH of water near an electrode interface may be appreciably lower due to enhanced ionization in the region of the surface electric field [5].

In computational studies, the influence of potential and electric field on a variety of substrates and for several reactions has been investigated by Wasileski et al. [6]. The orientation of adsorbed water depends on potential and field, generally resulting in the hydrogen atoms being oriented closer to the surface for more negative potentials and fields. In methanol dehydrogenation, the key step of first-hydrogen removal produces CH_2OH_{ads}, with progressively higher potentials favoring production of CH_3O_{ads}. These results fall in line with experimental observations of CH_2OH_{ads} in solution and CH_3O_{ads} in vacuum [7]. The influence of electric field on the decomposition of methyl groups on a Ni(211) surface was examined by Che et al. [8]. For successive dehydrogenation of $CH_{3,ads}$, both coadsorbate adsorption energies and reaction barriers increase with positive field.

Our previous studies of field-induced water ionization found a variety of protonated clusters $(H_2O)_nH^+$ with n varying from 1 to 10 [5,

* Corresponding author.
E-mail addresses: Chris.Rothfuss@wyoleg.gov (C.J. Rothfuss), stuve@uw.edu (E.M. Stuve).

http://dx.doi.org/10.1016/j.susc.2015.12.023
0039-6028/Published by Elsevier B.V.

9–11]. Ionization begins at a field of 0.3 V/Å with the production of clusters of $n \geq 4$. With increasing field, the cluster size decreases until only the $n = 1$ cluster is produced, which occurs at 1.2 V/Å [11].

In this study we examine the behavior of mixed water/methanol clusters in field ionization. From an applied point of view, the water/methanol system is central to a direct methanol fuel cell, in which methanol reacts at the anode in the overall process

$$CH_3OH_{elyte} + H_2O_{elyte} \rightarrow CO_{2gas} + 6\ H^+_{elyte} + 6\ e^-. \quad (2)$$

If, however, one were to include solvating water molecules, the reaction becomes

$$\left[(CH_3OH)(H_2O)_p\right]_{elyte} + (6n-p+1)\ H_2O_{elyte} \rightarrow CO_{2,gas} + 6\ \left[(H_2O)_nH^+\right]_{elyte} + 6\ e^-, \quad (3)$$

and the large water load of the reaction is evident. Methanol and water are completely miscible and exhibit complex hydrogen bonding behavior [12–17] and thermodynamic properties [18]. For a typical solvation shell for methanol of $p = 3$ [12] and for hydrogen of $n = 3$, the net number of water molecules processed in Eq. (3) is 19 per methanol molecule. This requires a lot of rearrangement of water at the anode surface.

From the fundamental point of view, cluster formation and size distributions of water/methanol mixtures are of inherent interest. The topic has received much study, but most of the hydrogen bonding details can be seen only in molecular dynamics (MD) simulations, of which a few references are [16–20]. A combined neutron-diffraction and MD study found various extended structures of hydrogen bonded molecules that occur over nearly the entire range of water/methanol compositions [19]. These structures include chains, sheets, and three-dimensional structures and are consistent with the increase in viscosity of water/methanol mixtures relative to the pure components. At low temperature (160 K), neutron diffraction measurements of methanol monohydrate in its crystalline form show that it has a hydrogen bond structure in which the hydrogen bond oscillates between the water-donor and hydroxyl-donor forms [14].

Previous mass spectrometry studies of methanol and methanol/water mixtures include pulsed field ionization [21], laser ionization [22,23], and secondary ion mass spectrometry [13]. These studies show (i) that pure methanol forms protonated clusters $(CH_3OH)_mH^+$ with $m \leq 4$ [13,21], (ii) that mixed clusters [n,m]; where n is the number of water molecules, m the number of methanol molecules, and the presence of H^+ in the cluster is assumed; form with n and m ranging from 1 to 3 [21], and (iii) that scission of the C–O bond occurs based on detection of CH_3^+ [13,22,23].

In this study we used pulsed field desorption time-of-flight mass spectrometry (TOF-MS) to investigate the field ionization behavior of methanol/water adlayers varying from pure water to nominally pure methanol on a Pt tip at 165 K. Pure and mixed clusters of water and methanol are identified and quantified to determine their fractional representation among desorbing ions. These results, examined as a function of composition, help identify ions that track the water content, the methanol content, or the combined water–methanol content. Time lags were observed for some of the peaks and are associated with cluster growth according to a two-step mechanism developed herein. The field dependence of pure methanol is also described.

2. Experimental methods

The system used in these experiments has been described previously [5,9,24]. It consisted of an ultrahigh vacuum system with a base pressure of 1×10^{-10} Torr and facilities for field emission microscopy (FEM), field ionization microscopy (FIM); pulsed field time-of-flight mass spectrometry, and velocity selector ($E \times B$) mass spectrometry. The experiments were performed on a Pt field emitter tip of radius 370 Å, determined by the best imaging field in Ne [25]. All measurements were conducted with the tip at 165 K.

A drift tube of nominally 1 m was used for the TOF measurements. Ions were detected by a microchannel plate capacitatively coupled to an Ortec 9308 picosecond time analyzer (PTA) for multichannel averaging. The PTA collected pulses in 1.25 ns time bins for flight times up to 40 μs in one pass. Data were collected and added in each bin for a total of 4000 passes, with a pass repetition rate of 400 Hz. The PTA data were subsequently boxcar averaged into 6.25 ns time bins to improve the signal-to-noise ratio. At the highest mass examined, mass 127 for $(H_2O)_7H^+$, there were 9 of the longer time bins within a single AMU, sufficient for minimal distortion of the data due to averaging. The results were then divided by 4000 to obtain the count rates per pass given in Figs. 2 and 3.

In general, field ionization studies are performed with positive tip potentials to avoid field emission of electrons that occurs at negative potentials. Consequently, all ions detected in pulsed field TOF are positive, meaning that some species often considered as anions, such as OH^-, will be detected as OH^+. As an example, field ionization of the dissociation fragments of methanol (discussed in Section 4.4) produces

$$CH_3OH_{ads} \rightarrow CH_3^+ + OH^+ + 2\ e^-_{tip} \quad (4)$$

with the two electrons that result from the two positive ions being transferred to the tip.

The tip was kept at 3000 V positive for all measurements to maintain a constant energy for the detected ions. A field was applied by a ring counter-electrode (CE) located near the tip. The CE was maintained at a constant, baseline potential of 2600 V positive and pulsed to initiate the TOF measurement. Pulses of 70 ns duration ranged from −300 to −900 V and were repeated at 400 Hz. The mass 19 $(H_2O)H^+$ peak was used to adjust for a time delay between the pulse and time of detection. The mass 37 $(H_2O)_2H^+$ peak was used to calibrate the length of the drift tube, which was determined to be 1.012 m.

Experiments were conducted for water/methanol partial pressures ranging from pure water to pure methanol. For the mixed layer experiments, the total pressure was maintained at 5×10^{-6} Torr for {H_2O:CH_3OH} ratios of {5:0} to {1:4}, where the numbers in brackets refer to the partial pressures of each species in units of 10^{-6} Torr. Pure methanol was dosed at a pressure of 6×10^{-6} Torr {0:6}. The water and methanol partial pressures were chosen to favor solvation by maintaining high species concentration at the surface.

Because the field induced adsorption properties of each species differ, the actual adsorbed composition need not be the same as the relative partial pressures. Adlayer composition was measured in these experiments, and good agreement was obtained between the relative partial pressures and actual composition for water mole fractions of 0.4 and greater. In field-free conditions, a temperature of 165 K would prevent the accumulation of multilayers. Because of field induced adsorption, however, we expect that multilayers were present, and that the amount of species removed by the pulse did not change the adsorbed amount significantly.

3. Results

3.1. Field ionization of adsorbed methanol

Fig. 1 shows TOF-MS results for field ionization of methanol as a function of pulse voltage. A number of ion clusters are evident with masses of 33, 65, 97, and 129. These correspond to methanol solvated proton clusters $(CH_3OH)_mH^+$, with m taking values of 1, 2, 3, and 4 in accord with the observed masses. The cluster of primary intensity decreases with increasing pulse voltage, from $m = 3$ at 300 V, to $m = 2$ at 400 V, and to $m = 1$ at 500 V. The decreasing cluster size with increasing ionization voltage is in agreement with our two-step field

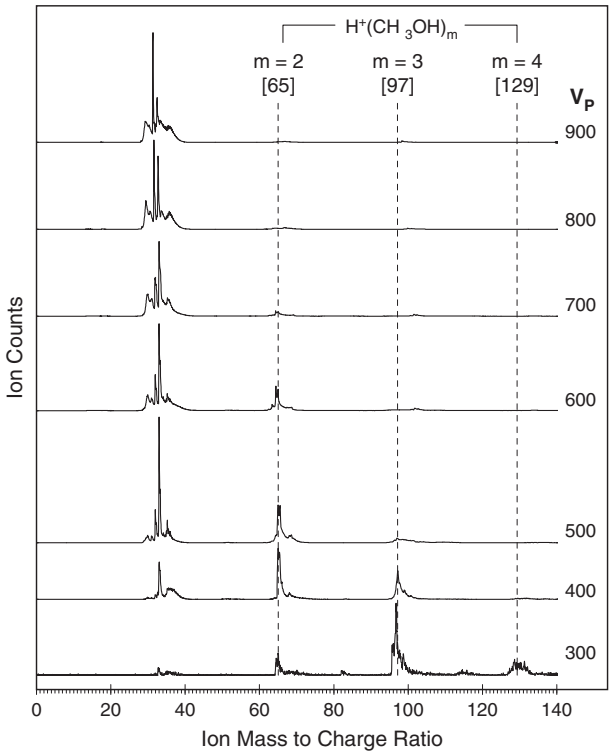

Fig. 1. Pulsed field desorption time-of-flight curves for 6×10^{-6} Torr methanol at 165 K for pulse voltages V_p ranging from 300 to 900 V. The baseline potential (between and during pulses) was 400 V. The range of fields (pulse plus baseline) varies from 0.38 to 0.70 V/Å. The peak heights are normalized for comparative purposes.

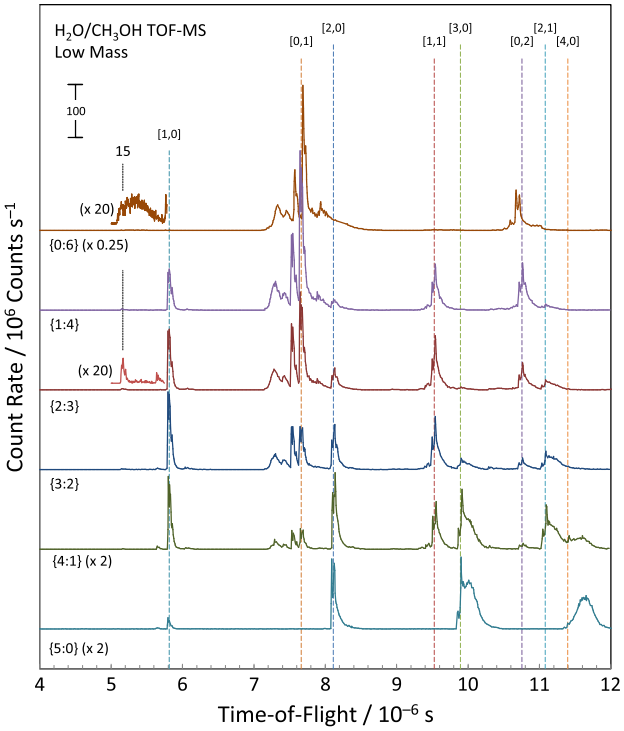

Fig. 2. Pulsed field desorption time-of-flight mass spectra for water/methanol mixtures as a function of composition at 165 K. The notation in brackets $\{p_w{:}p_m\}$ refers to the partial pressures of water (p_w) and methanol (p_m) in units of 10^{-6} Torr. The baseline and pulse potentials were 400 and 600 V, respectively, corresponding to a combined baseline and pulse ionization field of 0.54 V/Å.

ionization mechanism, in which smaller clusters require stronger fields for emission.

The peak for the $m = 1$ cluster (mass 33) is accompanied by peaks at masses 30, 31, 32, and 35. The first three of these can be assigned to H_2CO^+, CH_3O^+, and CH_3OH^+ or O_2^+, respectively. The only plausible species to which mass 35 can be assigned has the stoichiometry $H_3O_2^+$. On the basis of microcalorimetry measurements, Lew et al. [26] identified a water-hydroxyl complex $(D_2O\cdots OD)_{ads}$ as a stable species formed in coadsorbed D_2O and O on Pt(111). The mass 35 peak is therefore assigned to the analogous $(H_2O\cdots OH)^+$ ion, hereafter abbreviated as $H_3O_2^+$, following field ionization and desorption from the Pt tip. The excess oxygen required to form $H_3O_2^+$ must come from scission of the C–O bond in methanol, which is supported by a peak corresponding to mass 15 in Fig. 2. An interesting result is that the ratio of the mass 32 to 33 peaks increases with increasing pulse voltage. This result is discussed further in Section 4.2.

3.2. Field ionization of adsorbed methanol/water mixtures

Figs. 2 and 3 show, respectively, low mass and high mass TOF-MS data for mixed water/methanol layers as a function of composition. The TOF of each cluster is indicated by dashed vertical lines labeled [*n*,*m*]. For pure water, peaks appear for clusters [*n*,0] with *n* ranging from 1 to 7. The peak intensity is small for the [1,0] cluster, approximately equal for the [2,0] and [3,0] clusters, and steadily decreasing for larger clusters. There is a time lag for appearance of the larger clusters, which is discussed in Section 3.3. The [3,0] cluster is the most prominent on the basis of its integrated intensity, consistent with previous studies from our laboratory [11].

Cluster distributions as a function of adlayer composition are plotted in Fig. 4 for water-only clusters, Fig. 5 for methanol-only clusters, and Fig. 6 for mixed clusters. The data for these plots, as well as other species not shown, are given in Table 1. The plots show the fractional amount of a given ion emission relative to the total ion emission in each experiment. This adjusts for differing counts among experiments. For the *y*-axis, each cluster or other species contributes one count of the total ion count. The *x*-axis is the water

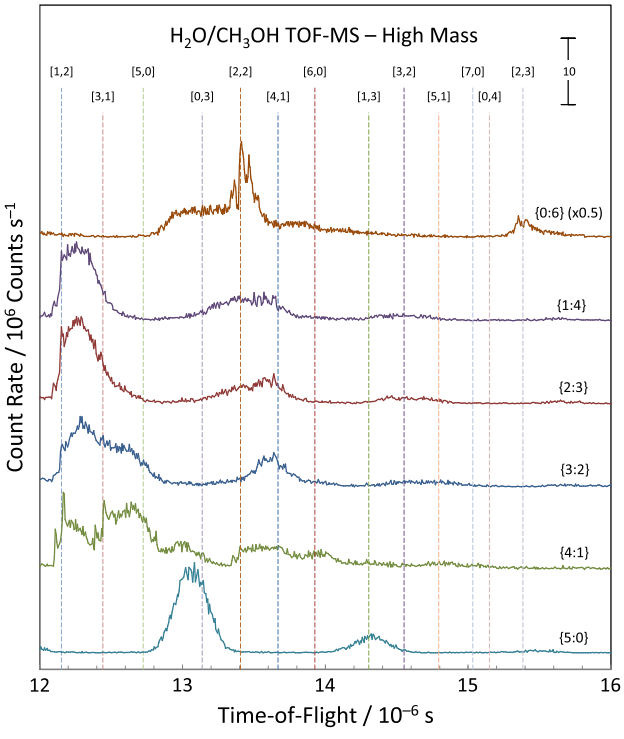

Fig. 3. Continuation of Fig. 2 to longer flight times.

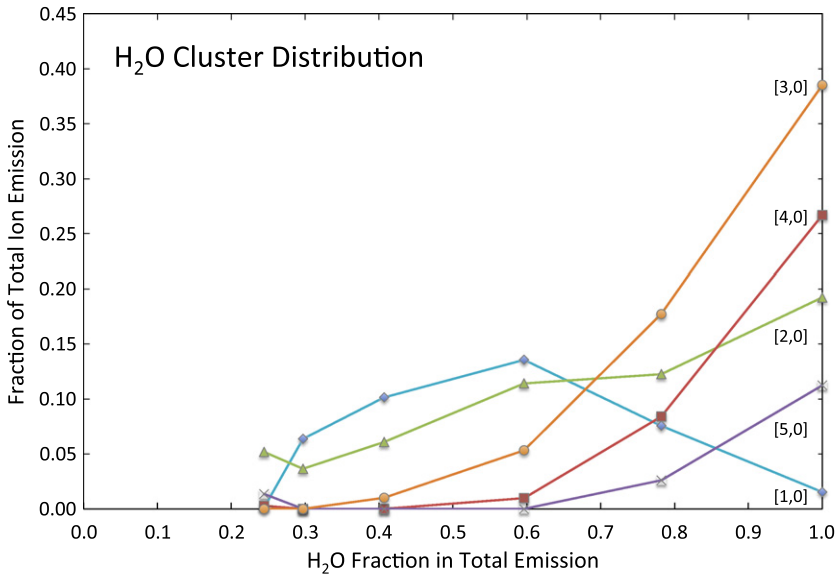

Fig. 4. Distribution of non-methanol containing water clusters [*n*,0] as a function of H_2O content in total emission. The *y*-axis is the fraction of each cluster of the total ion emission (including clusters containing methanol). The lines connect the data points and are guides to the eye.

composition determined by multiplying each cluster by the amount of water molecules in that cluster for all water containing clusters, and likewise for methanol. The result is an experimentally measured composition of the adlayer, listed in Table 1. Note, in Fig. 4, that the data points fall on the *x*-axis close to the compositions expected for water mole fractions of 0.4 and greater. For the {1:4} and {0:6} cases, significant amounts of water were detected in some of the clusters, as will be discussed below.

Fig. 4 shows that [*n*,0] clusters increase monotonically with water content for $n \geq 2$. A notable exception is the [1,0] cluster, which exhibits a maximum at a water fraction of 0.6 and decays to low values at the two extremes in composition. This result is discussed further in Section 4.3.

For the primary methanol related species, Fig. 5 shows that the [0,1] and [0,2] clusters decrease monotonically with increasing water content. So, too, do masses 32 (CH_3OH^+) and 35 ($H_3O_2^+$), although mass 32 is relatively constant for water mole fractions of 0.4 or less. Also shown is the behavior of mass 15 (CH_3^+). Although it is a minor species, it indicates that C–O bond scission occurs, which leaves OH and therefore a possibility for forming water or other species such as $H_3O_2^+$. The magnified portion above the {0:6} curve of Fig. 2 shows the TOF signal for mass 15 through the onset of mass 19. Signal is present for masses 15–18. The nature of the peak is different from that of the {2:3} curve, which shows only mass 15 (as does the {1:4} curve, not shown). The enhanced presence of O and OH species in the {0:6} curve is evidence for water production.

As expected, all of the primary mixed complexes exhibit maxima at intermediate water mole fractions and zero signal for the pure species, as shown in Fig. 6. The simplest mixed cluster, [1,1], is the most prominent for all cases except a water mole fraction of 0.8. At larger water

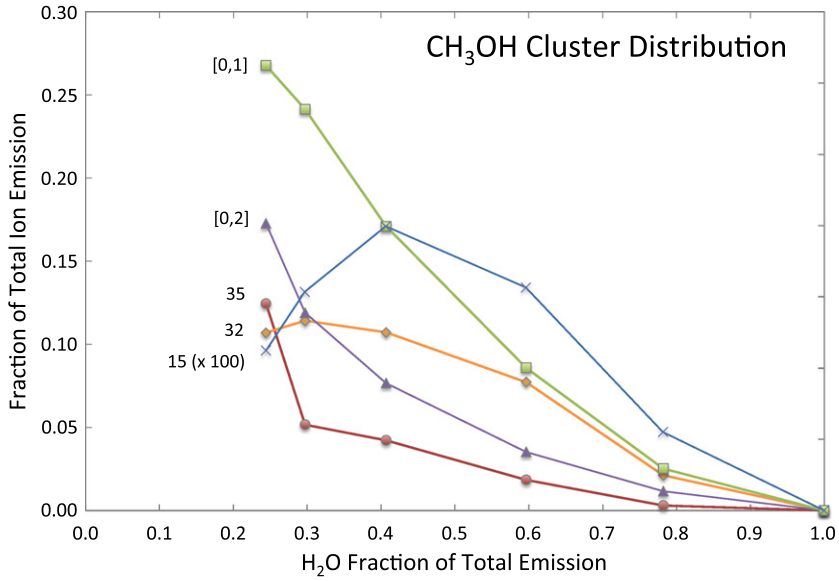

Fig. 5. Distribution of non-water containing methanol clusters [0,*m*] as a function of H_2O content in total emission. Also included are the distribution of mass 35 and 32 species. The lines connect the data points and are guides to the eye.

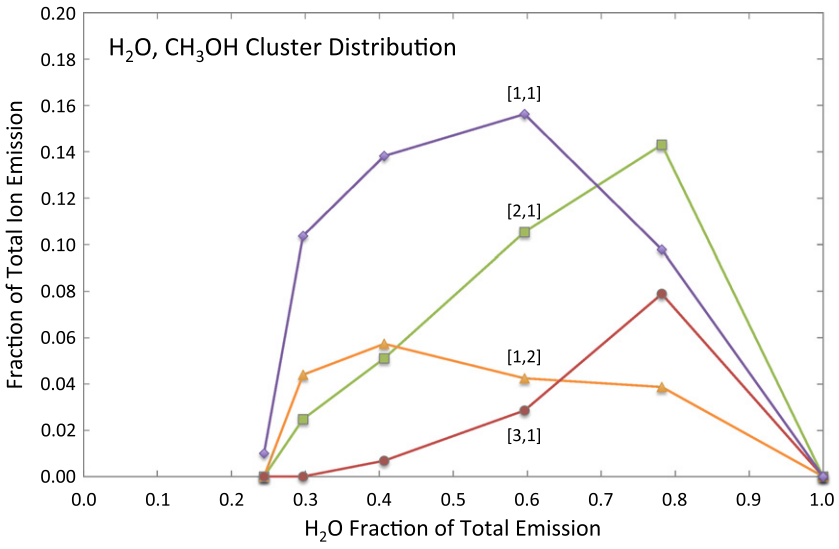

Fig. 6. Distribution of water/methanol clusters [*n*,*m*] as a function of H_2O content in total emission. The lines connect the data points and are guides to the eye.

content, clusters of multiple waters [2,1] and [3,1] are favored due to the high proportion of water. Conversely, lower water content favors the [1,1] and [1,2] complexes.

Table 1
Cluster ion counts normalized to the total ion count measured for each adlayer composition. The "Total Water" and "Total Methanol" rows give the amount of each molecule, accounting for multiple water or methanol molecules within a cluster, normalized to the total ion count. The "% Water" and "% Methanol" rows give the respective mole fractions of each species in the adlayer, as measured by TOF-MS. For clarity, values below 0.0005 are represented by a dash.

		H_2O:CH_3OH relative partial pressures					
H_2O:CH_3OH	Assignment	0:6	1:4	2:3	3:2	4:1	5:0
15 (× 100)	CH_3^+	0.112	0.154	0.200	0.157	0.055	–
16	O^+	0.002	–	–	–	–	–
17	OH^+	0.001	–	–	–	–	–
18 (× 100)	H_2O^+	–	–	0.001	0.002	0.003	0.001
19	[1,0]	0.001	0.064	0.101	0.135	0.076	0.015
21	HNe^+?	–	0.002	0.005	0.006	0.003	0.001
30	CH_2O^+, $C_2H_6^+$	0.105	0.090	0.080	0.057	0.018	–
31	CH_3O^+	0.063	0.038	0.032	0.027	0.007	–
32	CH_3OH^+, O_2^+	0.107	0.114	0.107	0.077	0.021	–
33	[0,1]	0.313	0.282	0.200	0.100	0.029	–
35	$H_3O_2^+$	0.125	0.052	0.042	0.019	0.003	–
37	[2,0]	0.052	0.036	0.061	0.114	0.123	0.192
51	[1,1]	0.010	0.104	0.138	0.156	0.098	–
55	[3,0]	–	–	0.010	0.053	0.177	0.385
65	[0,2]	0.173	0.119	0.077	0.035	0.012	–
69	[2,1]	–	0.025	0.051	0.105	0.143	–
73	[4,0]	0.003	–	–	0.010	0.084	0.267
83	[1,2]	–	0.044	0.057	0.042	0.039	–
87	[3,1]	–	–	0.007	0.029	0.079	–
91	[5,0]	0.014	–	–	–	0.026	0.113
97	[0,3]	0.020	0.011	0.009	–	–	–
101	[2,2]	0.006	–	0.015	0.023	0.033	–
105	[4,1]	–	0.012	–	–	0.017	–
109	[6,0]	–	–	–	–	–	0.023
115	[1,3]	–	0.005	0.003	0.003	–	–
119	[3,2]	–	–	0.003	0.004	0.010	–
123	[5,1]	–	–	–	–	–	–
127	[7,0]	–	–	–	–	–	0.003
129	[0,4]	0.005	–	–	–	–	–
133	[2,3]	–	–	–	–	–	–
Total		1	1	1	1	1	1
Total Water		0.335	0.440	0.655	1.137	2.141	3.344
Total Methanol		1.038	1.041	0.956	0.771	0.598	–
% Water		0.244	0.297	0.407	0.596	0.782	1.000
% Methanol		0.756	0.703	0.594	0.404	0.218	–

3.3. Time lag for clusters

All of the curves in Figs. 2 and 3 show evidence for time lags between the expected and actual arrival time for a given mass. Time lags are most evident for high masses, where emission becomes increasingly dependent on cluster growth. This effect is most apparent in the TOF data for pure water. Fig. 7 shows the signal for each water-only cluster plotted as a function of its time lag. The expected arrival time is zero and indicated by the dashed line. The signal at increasing time delay shows the distribution of actual arrival times. Table 2 lists all measurable time lags from these experiments.

Since the [1,0] and [2,0] arrival times are used to calibrate the instrument, the time delay of these species is defined as zero. (Alternatively, if the [1,0] and [0,1] clusters were used to calibrate the instrument, the result for the [2,0] cluster would be unchanged.) Both the [1,0] and [2,0] clusters have sharp peaks, as would be expected for an event with minimal surface processes prior to emission. When the [2,0] and [1,0] peaks are compared at equal peak height, it is evident that the [2,0] tail extends beyond that of the [1,0] peak, indicating that a small time lag occurs for a portion of the [2,0] cluster. The [3,0] cluster shows both a spike at zero time lag, and a peak at a time lag of 127 ns. Larger clusters show longer time lags, as indicated in Fig. 7.

The time lag is plotted as a function of cluster size in Fig. 8. The increase in time lag is monotonic with cluster size. The time lags for clusters $n = 3$ to 5 can be fit with a straight line of slope 110 ns per H_2O cluster molecule and zero time lag at $n = 2$. The time lags for clusters larger than $n = 5$ increase at a lesser rate.

4. Discussion

4.1. Ionization and cluster growth: the two-step mechanism

In spite of the large number of ionic clusters observed in these experiments, the number of reactions necessary for an explanatory mechanism can be reduced to just four types:

Ionization/neutralization

$$(HX)_n(HY)_m + HX|HY \underset{k_{neut}}{\overset{k_{ion}}{\rightleftharpoons}} [n,m]^+ \cdots X^-|Y^- \tag{5}$$

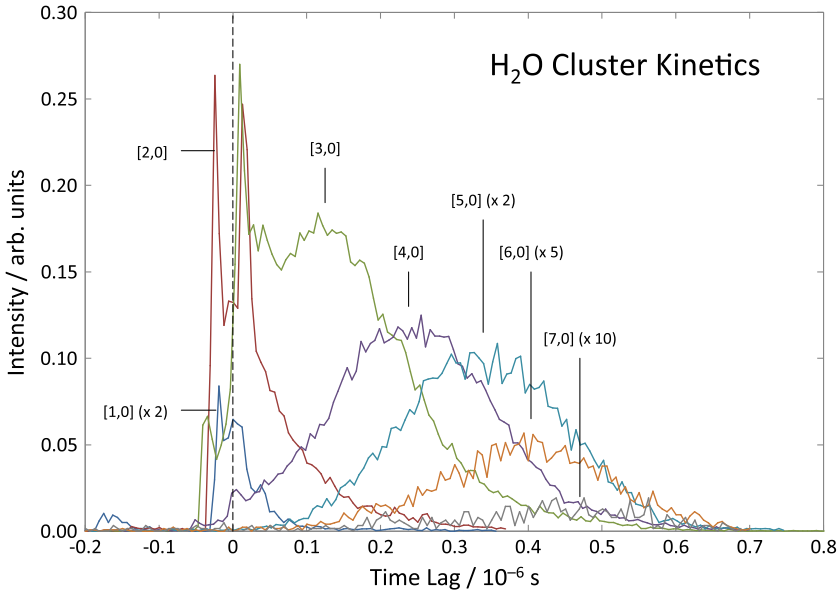

Fig. 7. Time lag after the field pulse for formation of H_2O clusters [n,0] as a function of cluster size n. The time of each peak maximum is indicated for clusters of $n = 3$ and larger.

Cluster growth and decay

$$[n,m]^+ + \mathrm{HX}|\mathrm{HY} \underset{k_{decay}}{\overset{k_{grow}}{\rightleftharpoons}} [n+1,m]^+|[n,m+1]^+ \tag{6}$$

Table 2
Mass assignments, expected arrival time, actual arrival time, and time lag for each species detected in the TOF-MS curves. Those species with equal or similar expected and arrival times are assigned a time lag of zero and given a blank entry. Since masses 19 and 37 are used in calibrating the instrument, their time lags are zero by definition, which is indicated by "Cal."

Mass	Assignment	Exp. time/μs	Act. time/μs	Time lag/μs
15	CH_3^+	5.166	5.166	
16	O^+	5.336	5.336	
17	OH^+	5.500	5.500	
18	H_2O^+	5.659	5.659	
19	[1,0]	5.814	5.814	Cal.
21	HNe^+?	6.113	6.113	
30	CH_2O^+, $C_2H_6^+$	7.306	7.306	
31	CH_3O^+	7.427	7.427	
32	CH_3OH^+, O_2^+	7.546	7.546	
33	[0,1]	7.663	7.663	
35	$H_3O_2^+$	7.892	7.892	
37	[2,0]	8.114	8.114	Cal.
51	[1,1]	9.526	9.526	
55	[3,0]	9.893	9.893	
65	[0,2]	10.754	10.72	−0.034
69	[2,1]	11.080	11.080	
73	[4,0]	11.397	11.53	0.133
83	[1,2]	12.153	12.25	0.097
87	[3,1]	12.442	12.56	0.118
91	[5,0]	12.725	13.05	0.325
97	[0,3]	13.138	13.53	0.392
101	[2,2]	13.406	13.8	0.394
105	[4,1]	13.669	13.92	0.251
109	[6,0]	13.927	14.31	0.383
115	[1,3]	14.305	14.51	0.205
119	[3,2]	14.551	14.73	0.179
123	[5,1]	14.794		
127	[7,0]	15.033	15.45	0.417
129	[0,4]	15.150	15.4	0.250
133	[2,3]	15.384		

Ion emission

$$[n,m]^+ \cdots \mathrm{X}^-|\mathrm{Y}^- | e^- \overset{k_{emit}}{\rightarrow} [n,m]^+_{gas} + \mathrm{X}^-|\mathrm{Y}^-|e^- \tag{7}$$

Discharge of ion fragments

$$\mathrm{X}^-|\mathrm{Y}^- \overset{k_{dis}}{\rightarrow} \mathrm{X}|\mathrm{Y} + e^-. \tag{8}$$

Here, X and Y are the fragments after ionization and represent OH and CH_3O (or CH_2OH). For convenience, a certain nomenclature has been invoked for this set of reactions. The strut | is to be read as "or," so the term HX|HY in Eq. (5) means "HX or HY," and likewise for subsequent uses of the symbol. The positive charge of the clusters is given explicitly by the "+" superscript, as in $[n,m]^+$, to illustrate that all reactions are charge-balanced. In the rest of this paper, the "+" superscript has been omitted, as it is obvious that the clusters must be positive. The triple dots symbol ⋯ represents an electrostatic interaction between the ionic cluster $[n,m]^+$ and the negatively charged fragment of ionization. This interaction may or may not be strong depending on the solvation shells around the cluster and $X^-|Y^-$. The ⋯ symbol can also represent interaction with the discharged electron in the metal. Finally, all species are assumed to be solvated, except the emitted ion $[n,m]^+_{gas}$, which is in the gas phase as indicated in Eq. (7).

Ionization, Eq. (5), initiates the process and may involve a single molecule or a cluster of molecules. Ionization adds a proton, while leaving the values of n and m unchanged. The ion cluster may interact with the ionized fragment (X^- or Y^-), though this interaction can change as the species solvate and diffuse away from each other. Clusters grow or decay as indicated in Eq. (6) and may involve addition (or removal) of HX or HY. Emission of the ion cluster, Eq. (7), requires surmounting the energy barrier required for breaking adsorption bonds and charge separation, leaving behind the ionized fragments or discharged electron in the metal. The ionized fragments discharge in Eq. (8) through a set of processes that may be rapid or prolonged according to the nature of reactions required for discharge. Ultimately, discharge results in an electron transferred to the metal. In water ionization, for example, the ionized fragment is OH^-, which, upon discharge, converts to O_{ads} [27].

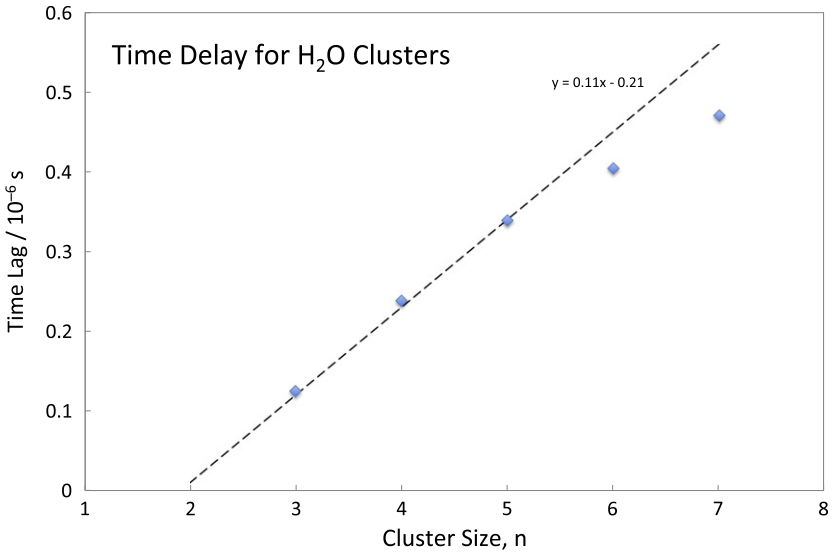

Fig. 8. Plot of time lag as a function of cluster size. The dashed line is a fit to the first three data points.

The kinetic rate constants in Eqs. (5)–(7) depend on the cluster, ionization fragments, and temperature, and a subset depend also an electric field. The dependencies are given as

$$k_{ion}, k_{neut}, k_{emit}, k_{dis} = f(n, m, \mathrm{X}, \mathrm{Y}, T, E) \tag{9}$$

$$k_{grow}, k_{decay} = f(n, m, \mathrm{X}, \mathrm{Y}, T). \tag{10}$$

The field dependence given in Eq. (9) follows from the existence of charge transfer, whether as ionization, neutralization, emission, or discharge. The absence of field dependence for growth and decay follows from the absence of charge transfer; the reactions involve only addition or removal of neutral species (HX or HY). As a general rule, the rate constants for a particular cluster size (for a single species $[n]$) depend on electric field as follows

$$k_{ion}^{[n]} < k_{ion}^{[n+1]} \tag{11}$$

$$k_{emit}^{[n]} < k_{emit}^{[n+1]}, \tag{12}$$

which means that a higher field is required both to ionize and to emit a smaller cluster [11]. The field dependence on emission can be explained in terms of ion solvation. Larger solvated clusters have greater screening of their ionic charge and therefore require less field for emission.

In general, it is not feasible to evaluate (that is, model) ionization data to obtain a set of rate constants, since even simple species require a large number of rate constants. For example, the [2,0] cluster of water requires 10 rate constants: one set of k_{ion}, k_{neut}, k_{grow}, k_{decay}, and k_{emit} each for $n = 1$ and $n = 2$. This assumes that the process stops after formation and emission of the [2,0] cluster. If the process were continued further to higher clusters, which is necessary to get an accurate model for the [2,0] cluster, then many more constants would be needed.

In interpreting field ionization, therefore, attention is focussed on two steps, growth/decay and emission, which make up the two-step model. Analysis is based on how each step changes with changing experimental conditions and how one step changes relative to the other. We shall now consider the two limiting cases of the two-step model: direct emission and indirect emission.

4.1.1. Direct emission

Direct emission consists of emission of the cluster immediately upon its formation by ionization. Cluster growth and decay are small processes in this limit. The conditions necessary for direct emission are:

$$\frac{k_{emit}}{k_{grow}} \gg 1 \tag{13}$$

$$K_{grow} \gg 1 \tag{14}$$

where $K_{grow} = k_{grow}/k_{decay}$ is the equilibrium constant for cluster growth. This set of conditions states that: (1) emission is facile relative to cluster growth and (2) cluster growth is favored over decay. This last condition is necessary so that a higher order cluster, which may be in indirect emission does not decay to the cluster of interest.

4.1.2. Indirect emission (cluster growth)

Indirect emission consists of ion clusters that can grow by adding solvating species prior to emission. Emission can occur for many different cluster sizes, but always occurs after at least one cluster growth step. The conditions necessary for indirect emission are:

$$\frac{k_{emit}}{k_{grow}} \lesssim 1 \tag{15}$$

$$K_{grow} > 1 \tag{16}$$

These conditions state that (1) cluster growth is preferred over emission, though emission is still possible and (2) cluster growth is favored over decay.

4.2. Field dependence of methanol ionization

Referring to Fig. 1, the largest clusters occur at the lowest fields. The methanol cluster of maximum intensity (peak and integrated) is [0,3] for $V_p = 300$ V. The [0,4] cluster occurs in smaller amounts, but is easily detected, nonetheless. In contrast, the [0,1] cluster, the simplest methanol cluster, is lower in intensity than the much more complex [0,4] cluster. This represents a case of low emission rate constants for the [0,1] and [0,2] clusters, that is, $k_{emit}^{[0,1]}$ and $k_{emit}^{[0,2]}$ are small relative to $k_{grow}^{[0,1]}$ and $k_{grow}^{[0,2]}$, respectively. The emission rate constant for the [0,3] cluster $k_{emit}^{[0,3]}$ is sufficiently large to maximize [0,3] emission, thereby starving the growth of higher clusters, as evident by the smaller intensities for [0,4] and higher clusters.

The influence of electric field on cluster distribution is readily apparent in Fig. 1. For pulse potentials V_p of 500 to 700 V, the dominant cluster shifts to [0,1]. This illustrates the field effects of both k_{ion} and k_{emit} given in Eqs. (11) and (12): smaller clusters are favored at higher fields because of increased ionization of smaller ions and increased emission of them, which prevents growth of larger clusters.

At the two highest potentials, however, the mass 32 peak exceeds the mass 33 peak for the [0,1] cluster due to direct ionization of methanol [21–23].

$$CH_3OH \rightarrow CH_3OH^+_{gas} + e^-. \quad (17)$$

This process does not require a two body ionization step as in Eq. (5), making it possibly a faster reaction, yet it does not have the solvation benefit that a cluster has to reduce the field needed for emission. At a sufficiently high field, where the energy benefit for solvation is superseded, direct ionization, rather than dissociative ionization [Eq. (5)], will be favored.

One point worth mentioning is the absence of CO formation in these experiments. While CO is a ubiquitous poison in electrocatalysis of methanol on platinum, its absence in these measurements can be attributed to the low temperatures and low fields employed. Formation of CO from methanol occurs at temperatures of 200 K and greater [28]. On the other hand, very high electric fields, greater than 2.2 V/Å, are required to form CO from methanol on a rhodium tip at 298 K [29].

4.3. Behavior of the [1,0] and [1,1] clusters in water/methanol adlayers

As seen in Fig. 4, the [1,0] cluster exhibits a maximum as a function of water mole fraction, whereas the other pure water clusters increase monotonically with increasing water mole fraction. The [1,0] cluster is a small fraction of the total ion emission for pure water, but for the {3:2} adlayer, it has maximum peak intensity and near maximum integrated peak intensity relative to all other peaks in the mass spectrum (Fig. 2).

The two-step mechanism sheds some light on this phenomenon in the sense that, since the field is the same for all of the experiments, the rate constants for ionization $k_{ion}^{[1,0]}$ and emission $k_{emit}^{[1,0]}$ should each remain the same in both the {5:0} and {3:2} adlayers. Less water is present in the {3:2} layer, however, so that the signal for the [1,0] cluster should *decrease*, rather than increase. A decrease was observed for the other water clusters. We propose, instead, that a methanol monohydrate ($CH_3OH \cdot H_2O$) forms in mixed water/methanol layers and that this species produces the [1,0] cluster by direct ionization, analogous to Eq. (17),

$$(CH_3OH \cdot H_2O) \underset{k^{[1,0]}_{neut^*}}{\overset{k^{[1,0]}_{ion^*}}{\rightleftharpoons}} [1,0]^+_{gas} + CH_3O^-, \quad (18)$$

where the direct ionization rate constant is signified by the asterisk in k_{ion^*}.

The crystal structure of per-deuterated methanol monohydrate has been studied with powder neutron diffraction at 160 K by Fortes [14]. Methanol and water interact by hydrogen bonding, as expected, but the hydrogen bond oscillates between a water-donor species ($DOD\cdots ODCD_3$) and the hydroxyl-donor species ($D_2O\cdots DOCD_3$), with each state having 50% occupancy according to symmetry requirements. While methanol/water solutions at room temperature exhibit long-range hydrogen bonding effects such as chains, sheets, and percolation structures [16,18–20], the limited mobility of methanol and water at low temperature would argue against such structures forming during low temperature deposition of the two species. The monohydrate form should therefore be more prevalent at the conditions of this experiment and especially so for nearly equimolar methanol/water mixtures. It is reasonable, then, to postulate its significance in field ionization of water/methanol mixtures.

Thus, the unusual behavior of the intensity of the [1,0] cluster follows from direct ionization of methanol monohydrate. The monohydrate is expected to have maximum concentration at equimolar mixtures of water and methanol, which agrees with the maximum in [1,0] cluster production at a water mole fraction of 0.6 (see Fig. 4). Indeed, [1,0] cluster production has similar functionality with respect to water mole fraction as do all of the mixed water/methanol clusters [*n*,*m*] (compare Figs. 4 and 6). Within this group, the best comparison is between the [0,1] and [1,1] clusters, which both have maximum production at a water mole fraction of 0.6. Finally, it should be noted that the decrease in the [0,1] cluster seen in Fig. 5 argues against its formation by direct ionization of methanol monohydrate.

4.4. Water production in methanol-rich adlayers

An overabundance of water was detected in strongly methanol-rich adlayers. This occurred for both the {1:4} and {0:6} adlayers, which have water mole fractions of 0.297 and 0.244, respectively, rather than the expected values of 0.25 and 0 (Table 1). This discrepancy in water content is too large to attribute to adsorption of background H_2O. The similarity of measured and expected water mole fractions for the other experiments (see Table 1) rules out a systematic error in estimation of water mole fractions. Hence, the unexpected values for the {1:4} and {0:6} cases should be considered valid.

Generation of water within the methanol adlayer requires scission of the C–O bond,

$$CH_3OH \rightarrow CH_3 + OH, \quad (19)$$

following which the CH_3 and OH groups can proceed to other species, including CH_3^+ and OH^+. The TOF results of Fig. 2 provide evidence of this, as mass 15 appears in all curves except that for {5:0} (see Table 1 for numerical values), and masses 16 and 17 occur only for the pure methanol case. Similarly small signals have been reported for laser ionization TOF-MS of methanol [22,23]. In contrast, a large signal for CH_3^+, nearly as large as that of the [0,1] cluster, was detected by TOF secondary ion mass spectrometry (TOF-SIMS) [13]. Though small, the signals for masses 15–17 imply that water can be produced within the methanol layer, as previously observed [22]. In forming other species, it is not necessary for CH_3 or OH to be present in significant quantities, only that they be highly reactive, which means that they would be detected as minor species. Once OH is formed, as in Eq. (19), a variety of reactions can ensue to make H_2O, which can then form clusters as in the water-rich cases.

The presence of oxygen-containing fragments can lead to other species that do not form from water. Chief among these is mass 35, for which the only reasonable assignment is $H_3O_2^+$. Mass 35 is the third most abundant species in the {0:6} data. Fig. 5 shows that it increases slowly from pure water, ending with a steep increase for the {0:6} case. The calculation of water content assumes that mass 35 results from water produced by methanol. Even if the mass 35 signal were attributed to methanol, however, the calculated water mole fraction would be 0.15, which is still too large to attribute to an artifact.

Regarding the fate of CH_3, it could ionize to CH_3^+ as seen in the TOF results, or combine with another CH_3 species to form $C_2H_6^+$, which would be detected as mass 30. Mass 30 can therefore be attributed to CH_2O^+ or $C_2H_6^+$. Other than the possibility of $C_2H_6^+$, there was no evidence for any C_2 or higher compounds. Alternatively, CH_3 could dehydrogenate to form CH_2 and lower species [8]. We saw no evidence for species ranging from mass 12 to mass 14, consistent with a low expectation of carbon formation on Pt.

4.5. Time lags in cluster formation

Time lags in the TOF spectra occur for all but one of the masses of 55 and above, as listed in Table 2 and evident in Figs. 3 and 7. The time lags range from 127 ns for the [3,0] cluster to 417 ns for the [7,0] cluster. The time lags for water vary systematically with cluster size, as shown in Figs. 7 and 8. As the [1,0] and [2,0] clusters were used to calibrate the instrument, their time delays are identically zero. They have sharp peaks, which indicate a spontaneous process, nonetheless. This is further verified by the peak at the onset of the [3,0] cluster, which aligns with zero time delay, although the bulk of the [3,0] signal exhibits an easily measurable delay. Fig. 8 shows that the time delay increases linearly with cluster size up to [5,0], with a smaller increase for the [6,0] and [7,0] clusters.

We attribute the time lag to cluster growth prior to emission, which is the indirect emission case discussed in Section 4.1.2. Alternative effects would be an energy deficit due to ionization in the homogenous phase or appearance potential. The smallest time lag of 127 ns corresponds to an energy deficit of 72 eV, which is well above typical values for either effect. The emission rate constants for small clusters are sufficiently small that water remains available to grow large clusters. Each of the cluster growth steps is kinetically limited, so the time delay increases with cluster size. The time lag provides information on the growth of the cluster to reach a given size. Other reactions, such as emission and cluster decay, affect the intensity of the TOF-MS peak, rather than the time lag. Thus, the time lag can be attributed to the growth rate in the manner

$$k_{grow}^{[n,0]} = \frac{1}{\Delta t_{[n,0]} - \Delta t_{[n-1,0]}} \quad \text{for} \quad n \geq 3 \tag{20}$$

where $\Delta t_{[n,0]}$ is the time lag of cluster [n,0]. In this manner, the growth rate constants for the [3,0], [4,0], and [5,0] clusters are each estimated as 9×10^{-6} s^{-1}, and those for the larger clusters are slightly higher.

In contrast to the broad, time-delayed TOF peaks of clusters [3,0] and higher, the peaks of the [1,0] and [2,0] clusters are sharp, only slightly wider than the pulse width, and occur without time delay. Cluster [3,0] also exhibits a sharp peak, as does [4,0], though only barely above the noise level. The sharp peak indicates that direct emission occurs and that cluster growth is a minor process. As discussed in Section 4.1.1, the direct emission pathway occurs when the rate constant for emission is much larger than that for growth. The distribution of the two direct emission peaks, that is, the low [1,0] peak and a much larger [2,0] peak, is controlled by the ionization rate constant $k_{ion}^{[n]}$. The field during the pulse, 0.54 V/Å, is sufficient to create $[2,0]^+$ and larger ions, but few $[1,0]^+$ ions, as indicated in Eq. (11).

5. Conclusions

Pulsed field time-of-flight mass spectrometry of water/methanol mixtures on a Pt field emitted tip at 165 K reveals a wide variety of protonated clusters of pure water, pure methanol, and mixed methanol/water. Water clusters $(H_2O)_nH^+$ with $n \leq 7$ were detected for a pure water adlayer, and methanol water clusters $(CH_3OH)_mH^+$ with $m \leq 4$ were detected for a nominally pure methanol adlayer. Mixed water/methanol adlayers produced most of the pure water and methanol clusters, as well as mixed clusters [n,m] of primarily [1,1], [2,1], [1,2], and [3,1], and higher clusters in small amounts. With one exception, the amounts of [n,0] and [0,m] clusters increased with the fraction of water or methanol, respectively, in the adlayer. The exception was the hydronium cluster [1,0], which peaked in intensity for approximately equimolar mixtures, coinciding with the composition-dependent behavior of all of the mixed clusters. This behavior is attributed to direct ionization of methanol monohydrate ($CH_3OH\cdot H_2O$) in methanol containing mixtures. Evidence for water production was observed in methanol-rich adlayers, such that a pure methanol adlayer could not be achieved. Water production was explained by C–O bond scission to produce CH_3 and OH, which, while detected only in small amounts, may play significant roles in water formation.

The TOF-MS data exhibited significant time lags for all of the masses above 55 but one. The time lags were most evident for pure H_2O and were analyzed in terms of a two-step mechanism involving a trade-off of ion cluster emission and growth of higher clusters. Direct emission peaks with no time lag occurred for the [1,0] and [2,0] clusters and partially for the [3,0] cluster. Time lags of approximately 110 ns per H_2O cluster molecule were observed for the $n = 3$ to 5 clusters, and the cluster growth rate constant was estimated as 9×10^6 s^{-1} for each of the corresponding species.

The field dependence of methanol pulsed field TOF revealed a behavior similar to that of pure water. At a field of 0.38 V/Å, the primary product is the $m = 3$ cluster with the $m = 2$ and 4 clusters detected in small amounts and the $m = 1$ cluster in trace amounts. Higher fields produced a shift to smaller clusters, with the $m = 1$ cluster dominating for fields of 0.49 to 0.59 V/Å. At larger fields the dominant ion was CH_3OH^+, produced by direct ionization of CH_3OH.

Acknowlegdements

We gratefully acknowledge support of this work by the Office of Naval Research. EMS: I am most grateful to my Ph.D. advisor, Prof. Robert Madix, for being able to share in his creativity, academic rigor, and depth of thought. It was my good fortune to be a part of his research group.

References

[1] F.T. Wagner, T.E. Moylan, Identification of surface hydronium: Coadsorption of hydrogen fluoride and water on platinum (111), Surf. Sci. 182 (1–2) (1987) 125.
[2] F.T. Wagner, T.E. Moylan, Generation of surface hydronium from water and hydrogen coadsorbed on Pt(111), Surf. Sci. 206 (1–2) (1988) 187.
[3] N. Kizhakevariam, E.M. Stuve, Coadsorption of water and hydrogen on Pt(100): formation of adsorbed hydronium ions, Surf. Sci. 275 (3) (1992) 223.
[4] H.J. Kreuzer, Physics and chemistry in high electric fields, Surf. Interface Anal. 36 (2004) 372.
[5] E.M. Stuve, Ionization of water in interfacial electric fields: An electrochemical view, Chem. Phys. Lett. 519–520 (0) (2012) 1.
[6] S.A. Wasileski, C.D. Taylor, M. Neurock, Modeling electrocatalytic reaction systems from first principles, Device and Materials Modeling in PEM Fuel Cells, Vol. 113 of Topics in Applied Physics, Springer-Verlag, Berlin 2009, p. 551.
[7] C. Taylor, S. Wasileski, J. Filhol, M. Neurock, First principles reaction modeling of the electrochemical interface: Consideration and calculation of a tunable surface potential from atomic and electronic structure, Phys. Rev. B 73 (16) (2006).
[8] F. Che, A.J. Hensley, S. Ha, J.-S. McEwen, Decomposition of methyl species on a Ni(211) surface: investigations of the electric field influence, Catal. Sci. Technol. 4 (11) (2014) 4020, http://dx.doi.org/10.1039/C4CY00406J.
[9] T.D. Pinkerton, D.L. Scovell, A.L. Johnson, B. Xia, V. Medvedev, E.M. Stuve, Electric field effects in ionization of waterâ¨ice layers on platinum, Langmuir 15 (3) (1999) 851.
[10] C.J. Rothfuss, V.K. Medvedev, E.M. Stuve, Temperature and field dependence of protonated water cluster emission from field adsorbed water layers on platinum, Surf. Sci. 501 (2002) 169.
[11] C.J. Rothfuss, V.K. Medvedev, E.M. Stuve, The influence of the surface electric field on water ionization: a two step dissociative ionization and desorption mechanism for water ion cluster emission from a platinum field emitter tip, J. Electroanal. Chem. 554–555 (2003) 133.
[12] M. Meot-Ner, Comparitive stabilities of cationic and anionic hydrogen-bonded networks, mixed clusters of water–methanol, J. Am. Chem. Soc. 108 (20) (1986) 6189.
[13] R. Souda, H. Kawanowa, M. Kondo, Y. Gotoh, Hydrogen bonding between water and methanol studied by temperature-programmed time-of-flight secondary ion mass spectrometry, J. Chem. Phys. 119 (12) (2003) 6194.
[14] A.D. Fortes, The crystal structure of methanol monohydrate $(CD_3OD)\cdot(D_2O)$ at 160 K from powder neutron diffraction, Chem. Phys. Lett. 431 (4–6) (2006) 283.
[15] G.M. Georgiev, K. Vasilev, K. Gyamchev, Hydrogen bonds in water–methanol mixture, Bulg. J. Phys. 34 (2007) 103.
[16] J.A. Batista da Silva, F.G.B. Moreira, V.M. Leite dos Santos, R.L. Longo, On the hydrogen bond networks in the water–methanol mixtures: topology, percolation and small-world, Phys. Chem. Chem. Phys. 13 (14) (2011) 6452.
[17] J.A.B. da Silva, F.G.B. Moreira, V.M.L. dos Santos, R.L. Longo, Hydrogen bond networks in water and methanol with varying interaction strengths, Phys. Chem. Chem. Phys. 13 (2) (2011) 593.
[18] J.-C. Soetens, P.A. Bopp, Water–methanol mixtures: Simulations of mixing properties over the entire range of mole fractions, J. Phys. Chem. B 119 (27) (2015) 8593.

[19] L. Dougan, S.P. Bates, R. Hargreaves, J.P. Fox, J. Crain, J.L. Finney, V. Réat, A.K. Soper, Methanol–water solutions: A bi-percolating liquid mixture, J. Chem. Phys. 121 (13) (2004) 6456.
[20] I. Bako, T. Megyes, S. Balint, T. Grosz, V. Chihaia, Water–methanol mixtures: topology of hydrogen bonded network, Phys. Chem. Chem. Phys. 10 (32) (2008) 5004.
[21] H.D. Beckey, Principles of field ionization and field desorption mass spectrometry, in: H. Frieser (Ed.), International Series in Analytical Chemistry, Pergamon Press, Oxford, 1977.
[22] T. Hatamoto, M. Okunishi, M. Matsumoto, T. Lischke, K. Shimada, G. Prümper, F. Kong, K. Ueda, Dissociative ionization of methanol in moderate intense laser fields, Chem. Phys. Lett. 434 (4–6) (2007) 205.
[23] M. Elshakre, Dissociative ionization of methanol in medium intense femtosecond laser field using time-of-flight mass spectrometry, Radiat. Phys. Chem. 112 (2015) 49.
[24] D.L. Scovell, T.D. Pinkerton, B.A. Finlayson, E.M. Stuve, The dielectric response of water in high electric fields: equilibrium water thickness and the field distribution, Chem. Phys. Lett. 294 (1998) 255.
[25] T.T. Tsong, Atom-probe field ion microscopy –Field ion emission and surface and interfaces at atomic resolution, Cambridge University Press, 1990.
[26] W. Lew, M.C. Crowe, E. Karp, O. Lytken, J.A. Farmer, L. Árnadóttir, C. Schoenbaum, C.T. Campbell, The energy of adsorbed hydroxyl on Pt(111) by microcalorimetry, J. Phys. Chem. C 115 (23) (2011) 11586.
[27] D.L. Scovell, T.D. Pinkerton, V.K. Medvedev, E.M. Stuve, Phase transitions in vapor-deposited water under the influence of high surface electric fields, Surf. Sci. 457 (2000) 365.
[28] N. Kizhakevariam, E.M. Stuve, Promotion and poisoning of the reaction of methanol on clean and modified platinum (100), Surf. Sci. 286 (3) (1993) 246.
[29] N. Kruse, G. Abend, J.H. Block, Observation of Rh-subcarbonyls on stepped Rh surfaces during catalytic reactions, J. Chem. Phys. 91 (1) (1989) 577.